Article

The Impact of Drought on Vegetation at Basin Scale: A Case Study of the Wei River Basin, China

Panpan Zhao [1,2], Qihui Chai [1], Bingbo Xie [3], Hongyang Li [1], Huicai Yang [4], Fang Wan [1,5,*] and Xudong Huang [1,2]

1   College of Water Resources, North China University of Water Resources and Electric Power,
    Zhengzhou 450045, China; zhaopanpan@ncwu.edu.cn (P.Z.); chaiqihui@ncwu.edu.cn (Q.C.);
    202103911@stu.ncwu.edu.cn (H.L.); huangxudong@ncwu.edu.cn (X.H.)
2   Hennan Key Laboratory of Water Resources Conservation and Intensive Utilization in the Yellow River Basin,
    Zhengzhou 450046, China
3   Ningbo Water Conservancy and Hydropower Planning and Design Institute Co., Ltd., Ningbo 315192, China;
    xiebingbo23@163.com
4   Academy of Eco-Civilization Development for Jing-Jin-Ji Megalopolis, Tianjin Normal University,
    Tianjin 300387, China; hcyang@tjnu.edu.cn
5   National Key Laboratory of Water Disaster Prevention, Nanjing Hydraulic Research Institute,
    Nanjing 210029, China
*   Correspondence: wanfang@ncwu.edu.cn

Abstract: Droughts in the Weihe River Basin are occurring more frequently and are becoming more intense. These events negatively affect industrial production, economic development, and ecosystems. Studying how vegetation changes in response to them is of practical significance. We report temporal and spatial trends in vegetation cover, use a copula function to analyze relationships between drought and vegetation cover, and assess the probability of vegetation loss in different drought scenarios. A vegetation index trends upwards from north to south in this basin; from 2001 to 2017, vegetation cover also trends upward in most areas, although it decreases in areas with high vegetation cover. An escalated susceptibility to drought has been observed in the southern and eastern sectors, where proximity to the riverbank correlates with heightened drought sensitivity, particularly in zones of intensified vegetation density. The probability of vegetation loss at the same vegetation loss preset point gradually increases with increased drought severity. These results will facilitate the formulation of countermeasures to prevent and combat the effects of drought on vegetation and land management.

Keywords: Weihe River Basin; meteorological drought; hydrological drought; vegetation cover change

1. Introduction

Terrestrial vegetation plays an important role in energy exchange, hydrological cycles, and climate regulation [1,2]. Changes in vegetation caused by climate change can be used to assess the impact of drought [3,4]. Drought is a widespread natural disaster [5], and prolonged drought can adversely affect ecosystems and social and national development [6]. With a changing climate, the severity, extent, and impact of a drought are increasing, especially in arid and semi-arid areas. Drought reduces water resources and decreases vegetation cover, and these impacts are becoming increasingly serious [7,8]. Therefore, the study of the interaction between drought and vegetation is currently a hot topic.

Due to the impact of climate change, precipitation-related events in China in the 21st century are becoming increasingly extreme, and the degree of drought may increase [9]. This trend is expected to exacerbate forest mortality attributed to drought [10]. At present, satellite remote sensing technology has been extensively leveraged within the realm of drought research, offering a robust analytical instrument for the surveillance and evaluation of arid events. Numerous scholars have engaged in deliberations regarding the utilization of remote sensing datasets for drought monitoring, articulating the existing accomplishments and prospective avenues for advancement [11,12]. They have postulated

potential future trajectories for the discipline, including the amalgamation of multi-source datasets, refinement of model precision, and the augmentation of real-time monitoring competencies [13]. Studies have shown that temperature rises are intensifying drought conditions in certain regions, affecting vegetation productivity [14], most studies have indicated a negative feedback mechanism between vegetation and drought, where an increase (or decrease) in vegetation corresponds to a weakening (or strengthening) of drought [15]. However, recent studies have suggested that vegetation may also enhance drought [16,17]. The normalized vegetation index (NDVI) has been used to quantitatively monitor dynamic changes in vegetation. It has become one of the most effective parameters to reflect vegetation cover and growth [18]. Zhou, et al. [19] used the Dynamic Reference Vegetation Cover Method (DRCM) to remove the influence of interannual variations in rainfall, with a focus on analyzing the impact of human activities on vegetation cover changes. Mu, et al. [20] examined inter-annual and inter-monthly changes in vegetation in different regions of inner Mongolia using rainfall and temperature data and reported that vegetation cover generally increased, with an east-high and west-low trend. Almouctar, et al. [21] reported a vegetation health index based on NDVI and land surface temperature in the Niger region and concluded that severe droughts had occurred in 2013 and 2019. In China, vegetation in most areas is positively correlated with drought, and the impact of drought on vegetation is mostly cumulative and particularly significant in arid and semi-arid regions [22]. Studying the combined effects of drought and land cover changes, such as deforestation and urbanization, on vegetation greenness and productivity can help predict the response of ecosystems to future environmental changes [23].

Many studies have investigated relationships between vegetation indices and indicators of drought. A common approach involves analyzing how vegetation growth sensitivity to drought varies across different time scales such as standardized precipitation evapotranspiration index (SPEI) to characterize drought conditions and normalized difference vegetation index (NDVI) to characterize vegetation changes [24]. In addition, some scholars use satellite remote sensing technology to monitor vegetation physiological changes and analyze how drought affects plant photosynthesis and transpiration [25]. Zuo, et al. [26] used remote sensing data, the combined deficit index (CDI) for agricultural drought assessment. Jiang, et al. [27] investigated the drought impact on vegetation with its spatio-temporal continuum. Guo, et al. [28] constructed a practical framework to fully assess socioeconomic drought dynamic risk. Shi, et al. [29] examined relationships between hydrology and meteorological drought based on coherent changes in wavelets, and reported a response relationship between hydrology and meteorological drought by calculating the EVI; by calculating lag-time correlation coefficients between EVI and the drought index, the response of vegetation to drought in the Huanghuaihai Basin was determined. Xu, et al. [30] constructed a coastal zone composite drought index based on rainfall, temperature, evapotranspiration, runoff, and normalized vegetation index data for the southeast coastal region, and, after comparing it with a standardized rainfall and Palmer drought indices, concluded that their new index was more suitable for monitoring drought in coastal regions. Copula functions have been extensively applied in hydrological analysis, effectively integrating remote sensing vegetation indices with ground-based drought data to statistically analyze the duration, intensity, and frequency of drought events. This technique reveals the spatiotemporal distribution characteristics of drought events and quantifies the relationships between different types of drought [31]. Copula functions offer a sophisticated statistical framework for the quantification of interrelations among different types of drought (for example, meteorological drought, hydrological drought, and agricultural drought) [32]. Additionally, Dixit and Jayakumar [33] proposed a novel approach based on copula functions to develop a multivariate drought index by combining various drought indicators. In the context of climate change, the application of copula functions has been expanded to study the relationships between vegetation cover changes and multiple meteorological factors [34]. When investigating the association between drought and vegetation cover changes, copula functions are utilized not only to quantify the dependency between vege-

tation indices and drought indicators but also to uncover the specific impacts of drought on vegetation cover.

The Weihe River Basin, a typical arid and semi-arid region in inland northwest China, is characterized by complex topography, geomorphology, and diverse climate. It is sensitive to climate change. Based on MODIS MOD13A2 data, we characterize spatial and temporal changes in vegetation cover in this basin. By calculating maximum correlations between different NDVIs and meteorological and hydrological drought indicator values at different time scales, we establish a binary joint distribution model based on the copula function to assess changes in vegetation cover under different drought scenarios. This model improves our understanding of the impacts of drought on vegetation cover over time and the vulnerability of ecosystems and provides a scientific basis for vegetation protection and management in the Weihe River Basin.

2. Study Area and Data Sources

2.1. Study Area Description

As the first major tributary of the Yellow River, the Weihe River originates from Bird Mouse Mountain in Weiyuan, Gansu, and flows through Gansu, Ningxia, and Shaanxi provinces (regions). The Wei River Basin (103–110° E, 34–38° N), with an 818 km total length and a basin area of 134,800 km^2, accounts for 18% of the Yellow River Basin [35] (Figure 1). The average annual water supply of the Weihe River Basin is about 11.056 billion m^3. The average annual natural runoff from the basin is 10.04 billion m^3, which accounts for 17.3% of the average annual natural runoff of the Yellow River Basin. Under similar rainfall conditions, the south bank of the Weihe River (20% of the total Weihe River Basin area) produces > 48% of all basin runoff [36,37]. Vegetation growth in this basin is closely related to climate, topography, and soil type; it is mostly grassland, broadleaf and coniferous forests, and crops [38].
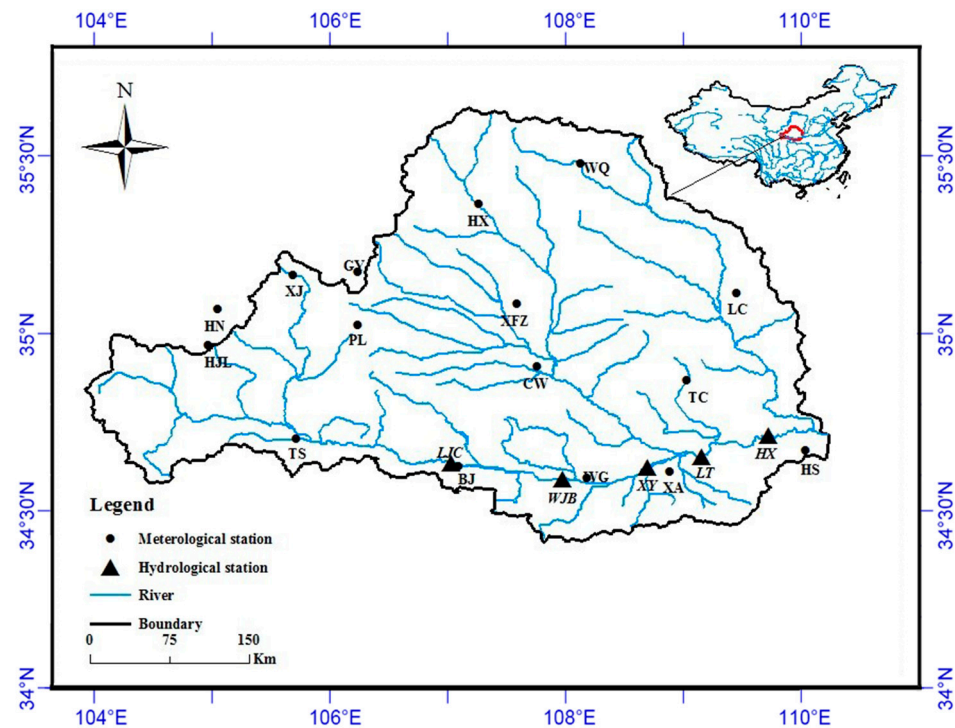

Figure 1. Study area, hydrological and meteorological stations in this study.

2.2. Data Sources

Base precipitation, runoff, and temperature data were provided by the China Meteorological Administration (https://www.cma.gov.cn/ (accessed on 9 July 2022)), Chinese

Academy of Sciences, and the Ministry of Water Resources, Soil and Water Conservation Association (http://loess.geodata.cn (accessed on 10 October 2022)). Data (monthly rainfall, day-by-day runoff data, and average temperature) from 13 meteorological stations (Pingliang, Huaxian, Huashan, Tianshui, Wugong, Xiji, Baoji, Xifengzhen, Changwu, Wuqi, Tongchuan, Xi'an, and Luochuan) were obtained from 1961 to 2017. The NDVI had a 1 km resolution, month-by-month NDVI dataset from China (January 2001 to December 2017), produced by a series of processing based on MODIS MOD13A2 data, and contains 264 TIF files (monthly maximum values of NDVI data from January 2001 to December 2017). NVDI data were obtained from the National Science and Technology Infrastructure Conditional Platform's National Geosystems Science Data Center (http://www.geodata.cn (accessed on 12 March 2023)). To characterize temporal and spatial changes in NDVI, analyze its response to drought, and eliminate the effect of winter snow, vegetation data for the growing season (March–November) were selected from 2001 to 2017. Month-by-month data were masked using ArcGIS software (version 10.2) to obtain vegetation data for the basin. Maximum value synthesis was performed to obtain annual average (growing season) NDVI data.

3. Methods

3.1. Vegetation Cover

Estimates of vegetation cover using the NDVI were made using a model based on the image element dichotomous model of Miaomiao [39]. This model assumes that there are only two watershed surfaces (vegetated and non-vegetated) and that the ratio of the area of the two in the image element is the weight, with the percentage of the pixel covered by vegetation indicating the vegetation cover degree of that pixel. [40,41]. The expression of vegetation cover FVC is presented in Equation (1):

$$FVC = (NDVI - NDVI_{Soil})/(NDVI_{Veg} - NDVI_{Soil}) \tag{1}$$

where $NDVI_{Veg}$ is pure vegetation partial cover, and $NDVI_{Soil}$ is pure bare soil partial cover [42]. Under ideal conditions, the FVC of pure vegetation is approximated to be 100%, and the FVC of pure bare soil is approximated to be 0, obtained as $NDVI_{Soil} = NDVI_{min}$, $NDVI_{Veg} = NDVI_{max}$, $NDVI_{max}$, and $NDVI_{min}$ are the two maximum and minimum values of NDVI in the region, respectively. To eliminate some unavoidable effects, we select the maximum and minimum values of the 5% confidence range.

3.2. Meteorological Drought Index and Hydrological Drought Index

3.2.1. Meteorological Drought Index

In 1993, the Standardized Precipitation Index (SPI) developed by McKee, et al. [43] was initially employed to characterize meteorological drought in Colorado, USA. Its widespread adoption can be attributed to its methodological simplicity, robust statistical properties, and its capacity to provide a normalized measure of drought across varying climatic regimes. Nalbantis and Tsakiris [44] documented the meteorological drought at multiple time scales by using SPI with hydrological years. The calculation method is as follows:

$$R_{i,j} = \sum_{j=1}^{3k} P_{i,j} \quad i = 1,2,3\cdots n \quad j = 1,2\cdots 12 \quad k = 1,2,3,4 \tag{2}$$

where $R_{i,j}$ is the accumulated rainfall, *i* represents the hydrological year, and *j* represents the first hydrological year.

$$SPI_{i,k} = \frac{R_{i,k} - \overline{R_k}}{S_k} i = 1,2,3\cdots n \quad k = 1,2,3,4 \tag{3}$$

where $\overline{R_k}$ and S_k are the mean and standard deviation of accumulated rainfall under the kth time scale, respectively.

Or

$$W_{i,k} = \ln\left(R_{i,j}\right) \quad i = 1,2,3 \cdots n \quad k = 1,2,3,4 \tag{4}$$

$$SPI_{i,k} = \frac{W_{i,k} - \overline{W_k}}{S_k} \quad i = 1,2,3 \cdots n \quad k = 1,2,3,4 \tag{5}$$

where $\overline{W_k}$ and S_k are the mean and the standard deviation of this logarithmic, respectively.

The classification of meteorological droughts based on Nalbantis and Tsakiris [44] was also used in this study: non-drought (SPI ≥ -0.5), mild drought ($-1.0 \leq$ SPI < -0.5), moderate drought ($-1.5 \leq$ SPI < -1.0), severe drought ($-2.0 \leq$ SPI < -1.5), and extreme drought (SPI < -2.0).

3.2.2. Hydrological Drought Index

Expanding upon the foundational concepts of the Standardized Precipitation Index (SPI), Nalbantis [45] introduced the Streamflow Drought Index (SDI) to empirically validate hydrological data from two distinct river basins in Greece. The SDI has since been widely recognized as a pivotal indicator for quantifying hydrological drought conditions. The computation of the SDI is delineated by the following formula:

$$V_{i,j} = \sum_{j=1}^{3k} Q_{i,j} \quad i = 1,2,3 \cdots n \quad j = 1,2 \cdots 12 \quad k = 1,2,3,4 \tag{6}$$

$$SDI_{i,k} = \frac{V_{i,k} - \overline{V_k}}{S_k} \quad i = 1,2,3 \cdots n \quad k = 1,2,3,4 \tag{7}$$

Or

$$y_{i,k} = \ln\left(V_{i,j}\right) \quad i = 1,2,3 \cdots n \quad k = 1,2,3,4 \tag{8}$$

$$SDI_{i,k} = \frac{y_{i,k} - \overline{y_k}}{S_k} \quad i = 1,2,3 \cdots n \quad k = 1,2,3,4 \tag{9}$$

where $V_{i,j}$ is the accumulated runoff, and $\overline{y_k}$ and S_k are the mean and variance of the accumulated rainfall under logarithmic operation, respectively. The classification of hydrological droughts was as follows: no drought ($0.0 < SDI$), mild drought ($-1.0 \leq SDI < 0.0$), moderate drought ($-1.5 \leq SDI < -1.0$), severe drought ($-2.0 \leq SDI < -1.5$), and extreme drought ($SDI < -2.0$).

For a comprehensive elucidation of the computational methodologies pertaining to the Standardized Precipitation Index (SPI) and the Streamflow Drought Index (SDI), Zhao, et al. [46] and Zhao, et al. [47] offer authoritative insights and methodological frameworks

3.3. Linear Regression Trend Analysis

To analyze changes in vegetation cover throughout Weihe River Basin from 2001 to 2017, interannual trends in change were fitted image-by-image elements using linear trend analysis in accordance with Equation (2):

$$\theta_{slope} = \frac{n \times \sum_{i}^{n} i \times NDVI_i - \sum_{i=1}^{n} i \times \sum_{i=1}^{n} NDVI_i}{n \times \sum_{i=1}^{n} i^2 - \left(\sum_{i=1}^{n} i\right)^2} \tag{10}$$

where θ_{slope} is the slope of the regression, n is the time span of the study (17 years), i is the ith year among 1–n years, and $NDVI_i$ is the mean value of NDVI in the ith year. Combining the slope of the trend and *p*-value, the trend in NDVI was categorized as significantly increasing ($\theta_{slope} > 0, p < 0.05$), significantly decreasing ($\theta_{slope} < 0, p < 0.05$), or with no significant change ($p > 0.05$).

3.4. Pearson's Correlation Coefficients

$$r = \frac{\sum_{i=1}^{n}(X_i - \overline{X})(Y_i - \overline{Y})}{\sqrt{\sum_{i=1}^{n}(X_i - \overline{X})^2}\sqrt{\sum_{i=1}^{n}(Y_i - \overline{Y})^2}} \tag{11}$$

where r is the correlation coefficient; X_i and Y_i are drought indicator and NDVI values, respectively; $\overline{X}$ and $\overline{Y}$ are mean values, *r* is in the range of $[-1, 1]$, with $r < 0$ indicating a negative correlation and $r > 0$ indicating a positive correlation.

3.5. Copula Function

Copula functions, as tools for constructing multivariate joint distributions with best-fitting marginals, can describe complex structures such as nonlinearities and asymmetries, and can also construct joint distributions of variables independent of the type of marginal distribution [48]. Copula functions have been widely used in various disciplines through multivariate modeling of variables and associated probabilistic prognostications (e.g., in flood frequency and drought risk analysis, runoff and climate modeling prediction, and financial risk and energy) [49,50]. Copula function C is a multivariate (k)-distribution function with marginal distribution on the interval $[0, 1]^k$ [51]. The specific functional form is expressed in Equation (12):

$$F(x_1, x_2, \ldots, x_k) = C(F_1(x_1), F_2(x_2), \ldots, F_k(x_k)) = C(u_1, u_2, \ldots, u_k) \tag{12}$$

where $F_k(x_k)$ represents the cumulative distribution function of the sequence x_k, the marginal distribution function (u_k).

The marginal distributions of variables were fitted using copula functions, choosing the commonly used normal [52], T [53], Gumbel [54], Frank [55], and Clayton [56] functions (Table 1). Optimal copula functions were fitted according to Kendall and Spearman rank correlation coefficients [57]. The optimal copula function was then applied, with the joint distribution between the two expressed as in Equation (13):

$$(P \leq porD \leq d, N \leq n) = F_{PorD,N}(pord, n) = C\left(u_{pord}, v_n\right) \tag{13}$$

where $C(\ )$ denotes the copula function; F denotes the cumulative distribution probability of the functional distribution; and u_{pord} and v_n denote the cumulative marginal distribution function of hydrological drought or meteorological drought and vegetation cover, respectively.

Table 1. Copula functions and their characteristics.

Copula	Copula Function $C(u,v,\theta)$	Generating Element	Parameter
Normal	$\varphi_{\theta,\rho}\left(\varphi^{-1}(u), \varphi^{-1}(v)\right)$	/	$(-1, 1)$
T	$t_{\theta,k}\left(t_k^{-1}(u), t_k^{-1}(v)\right)$	/	$(-1,1)k > 0$
Clayton	$\left(u^{-\theta} + v^{-\theta} - 1\right)^{-1/\theta}$	$\left(t^{-\theta} - 1\right)/\theta$	$(0, +\infty)$
Frank	$-1/\theta\left[\ln\left(1 + \left(e^{-\theta u} - 1\right)\left(e^{-\theta v} - 1\right)\right) - \ln\left(e^{-\theta} - 1\right)\right]$	$\ln\left(e^{\theta t} - 1\right) - \ln\left(e^{\theta} - 1\right)$	$(-\infty, +\infty)$
Gumbel	$exp\left[\left(-\left((-\ln u)^{\theta} + (-\ln v)^{\theta}\right)\right)^{1/\theta}\right]$	$(-\ln t)^{\theta}$	$[1, +\infty)$

Using the optimal copula function, a correlation dependence model between drought and change in vegetation cover was established. The conditional probability magnitude of vegetation state under different degrees of drought was deduced. The conditional

probability that a vegetation state was lower than a preset point (0.5, 0.3, 0.1) under different drought scenarios (*SPI* < *spi* or *SDI* < *sdi*) is expressed as in Equation (14):

$$
\begin{aligned}
P(NDVI < ndvi \quad &|SPI < spi \ or \ SDI < sdi) \\
&= \frac{P(NDVI<ndvi, SPI<spi \ or \ SDI<sdi)}{P(SPI<spi \ or \ SDI<sdi)} \\
&= \frac{F_{SPI \ or \ SDI, \ NDVI}(ndvi, spi \ or \ sdi)}{F_{SPI}(spi \ or \ sdi)}
\end{aligned}
\tag{14}
$$

It also allows for more accurate drought conditions, in accordance with Equation (15):

$$
\begin{aligned}
P(NDVI < ndvi \quad &|spi_0 < SPI < spi_1 \ or \ sdi_0 < SDI < sdi_1) \\
&= \frac{P(spi_0<SPI<spi_1 \ or \ sdi_0<SDI<sdi_1, NDVI<ndvi)}{P(spi_0<SPI<spi_1 \ or \ sdi_0<SDI<sdi_1)} \\
&= \frac{F(spi_1 \ or \ sdi_1, ndvi) - F(sdi_0 \ or \ sdi_0, ndvi)}{F_{SPI \ or \ SDI}(spi_1 \ or \ sdi_1) - F_{SPI \ or \ SDI}(spi_0 \ or \ sdi_0)}
\end{aligned}
\tag{15}
$$

We considered three levels of drought: the probability of loss of vegetation status below 0.5 (moderate), 0.3 (severe), and 0.1 (extreme).

During a drought, researchers will focus on the condition of vegetation in a transient drought phase and therefore set the conditional probability density function for the case where *SPI* = *spi* or *SDI* = *sdi*, as in Equation (16):

$$
F_{NDVI \leq ndvi}(ndvi|spi \ or \ sdi) = c(F_{NDVI}(ndvi), F_{SPI \ or \ SDI}(spi \ or \ sdi)) \cdot F_{NDVI}(ndvi)
\tag{16}
$$

where c( ) denotes the copula joint density function of F_{NDVI} and $F_{SPI \ or \ SDI}$. It is possible to integrate the area at *NDVI* < *nvdi* so that the probability of change in vegetation cover can be obtained for a given scenario.

4. Results

4.1. Characteristics of Spatial and Temporal Distribution of NDVI

The NDVI changed significantly in different regions of the Weihe River Basin (Figure 2). NDVI values trended upwards from north to south, peaking at 0.72 and lowest at 0.04. To better understand the spatial distribution and quantitative changes in NDVI from 2001 to 2017, average NDVI values for the last 20 years were calculated using image elements as a unit of calculation; NDVI was reclassified into four classes and the proportion of NDVI image elements in different regions was obtained (Figure 2b). From the spatial map of NDVI class distribution, the proportion of NDVI image elements in the Weihe River Basin was mostly concentrated in 0.20–0.40 (mainly in the northern and western region, 45% of the basin area) and 0.40–0.60 (mainly in the central and southern region, accounting for 46% of the basin area). Basin topography is complex, including plains, mountains, and hills, and different vegetation distribution types occur, leading to differences in the spatial distribution of NDVI.
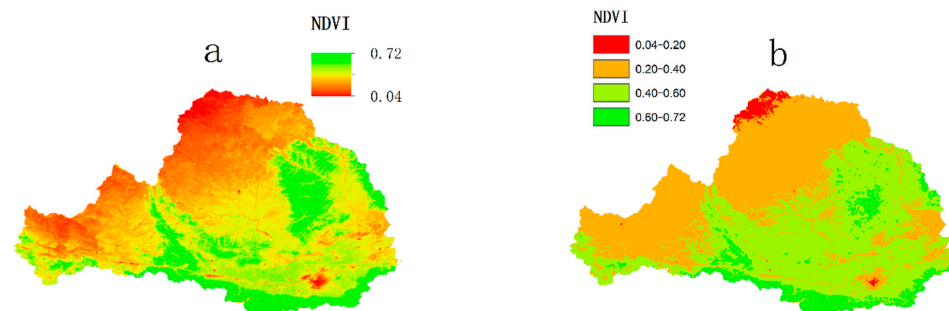

Figure 2. Average NDVI spatial distribution of Wei River Basin, 2001–2017: (**a**) spatial distribution of NDVI; (**b**) NDVI grading map.

The upward trend (~0.05 decade^{-1}) in annual mean NDVI from 2001 to 2017 is shown in Figure 3. Mean NDVI differs annually, possibly because of climate, but also because of a policy to return farmland to forests.
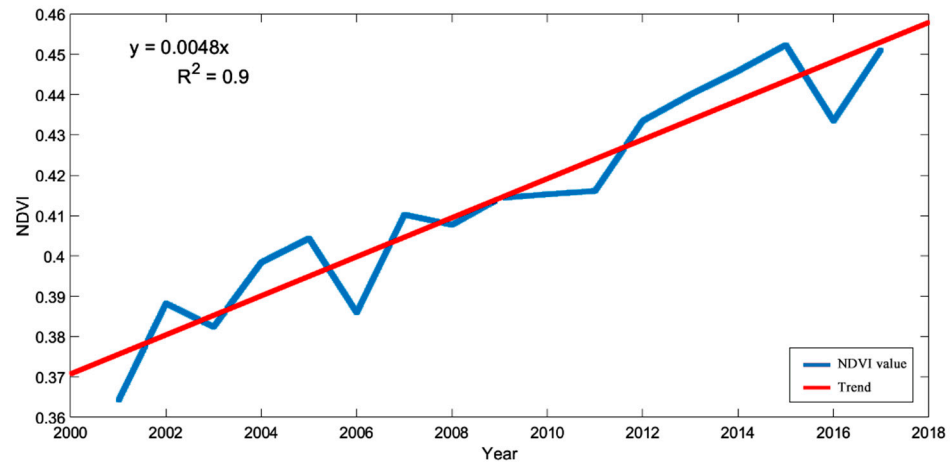

Figure 3. Trends in average annual NDVI for Weihe River Basin, 2001–2017.

4.2. Characteristics of Spatiotemporal Variations in Vegetation Cover Changes

The distribution of average vegetation cover from 2001 to 2017 is shown in Figure 4. Average vegetation cover varies significantly, annually; cover is high in the east and south, and low in the west and north. Areas with higher vegetation cover occur mainly in the northern foothills of Qinling Mountain, and on Liupan, Ziwuling, and Huanglong mountains, where land is mostly forested. Areas with lower vegetation cover occur mainly in barren and sparse grasslands in the northwestern watershed. Vegetation cover throughout this basin may vary because of local natural environments. The climate in the eastern and southern basins is favorable for crop growth, so land cultivation rates and vegetation cover are high (mostly between 0.7 and 1.0); most of the western and northern basins occur on the Loess Plateau, where precipitation is low, the climate is arid, deserts are common, and vegetation cover is low (mostly between 0 and 0.3).
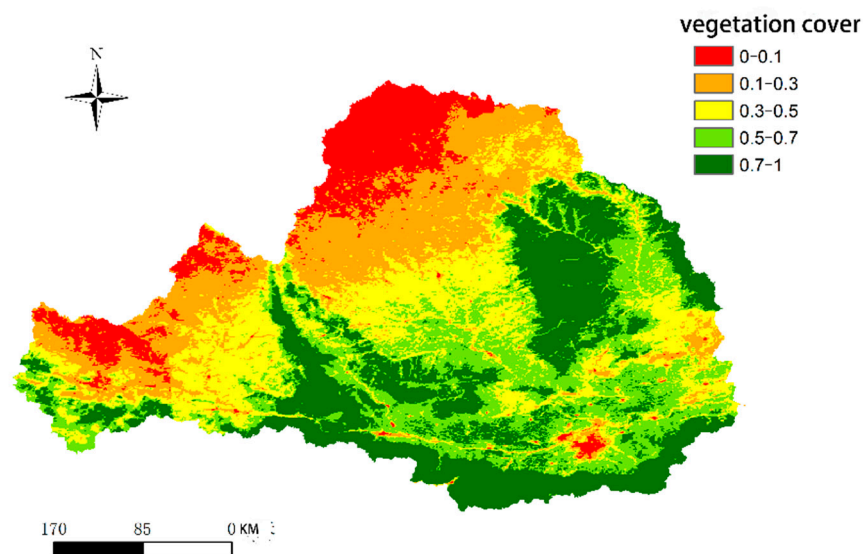

Figure 4. Distribution of average vegetation cover in Wei River Basin, 2001–2017.

Over time, vegetation cover trended upwards mostly in the northeast, central, and most of the southwestern and northwestern areas of the basin (Figure 5). To quantify this

change, the area and percentage of each type of change were calculated (Table 2). Areas that trended upwards accounted for 55.26% of the total watershed area, with significant increases occurring in 16.13% of the entire watershed (21,800 km^2) and non-significant increases occurring in 39.13%. Areas with significant decreases accounted for 10.37% of the watershed area (14,000 km^2), and areas with non-significant decreases accounted for 34.37% (46,300 km^2). The percentage of land on which trends in vegetation cover increased and decreased was similar. Compared with the spatial distribution of annual average vegetation cover, areas with high annual average vegetation cover had a tendency to decrease over time, and those areas with low vegetation cover coverage tended to increase over time, possibly because of local agricultural cultivation and ecological policies.
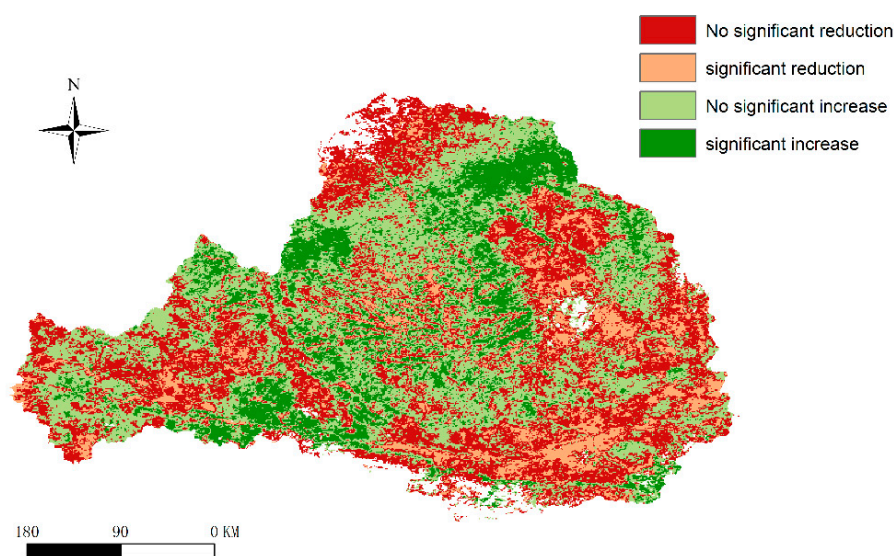

Figure 5. Distribution of changes in vegetation cover in Weihe River Basin, 2001–2017.

Table 2. Trends in vegetation cover, Weihe River Basin, as a percentage of watershed area.

Form	Area (km^2)	Proportion of Watershed (%)
No significant reduction	46,300	34.37
No significant increase	52,700	39.13
Significant reduction	14,000	10.37
Significant increase	21,800	16.13

4.3. Correlation Between NDVI and Drought

The effect of drought on NDVI was investigated by calculating Pearson's correlation coefficients between annual average NDVI and SPI and SDI values over a 12-month period in accordance with Equation (3).

The distribution of correlation coefficients between annual average NDVI and annual-scale drought indicator values (SPI and SDI) from 2001 to 2017 is presented in Figure 6. The annual average NDVI was significantly and negatively correlated with SPI and mainly occurred in the southern and western parts of the basin. Correlation coefficients between the basin's multi-year average NDVI and SDI were negative and mainly occurred in the southern part of the basin. Areas with negative correlations between the two occurred mostly in the same areas in the basin, possibly because of topography and vegetation type. Because areas with negative correlations were mostly on plains, where most vegetation was cultivated, cover in these areas may be related to agriculture; NDVI values of vegetation also correlated highly with human activities.
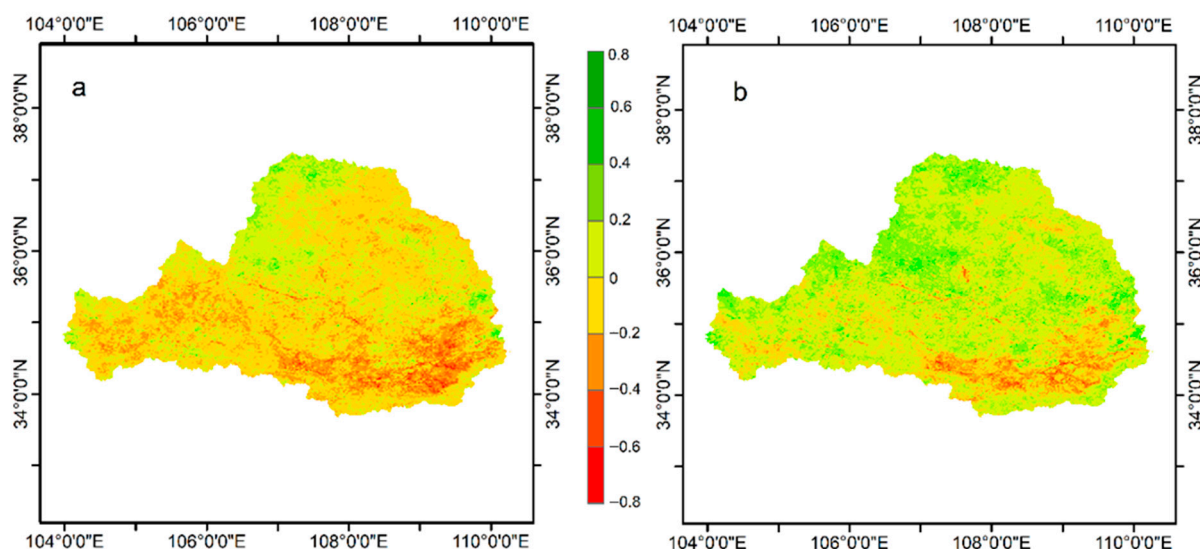
Figure 6. Spatial distribution of r_(SPI-NDVI) (**a**) and r_(SDI-NDVI) (**b**) in Weihe River Basin, 2001–2017.

4.4. Analysis of Correlations Between Changes in Vegetation Cover and Drought Scales

The response of vegetation to changes in water regime differs during the growing season, because during this time vegetation grows vigorously, water demand is high, and plants are sensitive to drought. During the non-growing season, growth is less vigorous and water demand is reduced. Accordingly, we selected vegetation during the growing season (March–November) for study. To investigate correlations between the effects of drought and vegetation cover over different lengths of time, meteorological or hydrological drought (SPI-3, SPI-6, SPI-9, SPI-12, or SDI-3, SDI-6, SDI-9, and SDI-12) sequences were subjected to Pearson's correlation analysis with growing season NDVI sequences (Figures 5 and 6). Differences in the effects of drought on vegetation occur at different time scales. Based on changes in vegetation cover, the response time of vegetation to drought can be determined. Because meteorological and hydrological drought over a 3-month period of time more closely affect vegetation, vegetation responds to drought in about 3 months; the close relationship between drought and vegetation state tends to slow down with increased time.

To better study seasonal differences in the effects of drought on vegetation, to establish a foundation for the distributions of drought and vegetation using copula functions, and to simulate the probability distribution of changes in vegetation cover under different drought conditions, Pearson correlation analysis was performed between monthly scale NDVI series and drought series at different time scales. Line graphs of correlations between drought and monthly scale NDVI for different drought durations are shown in Figure 7. Correlation coefficients between NDVI in spring and drought index values for each time scale gradually increased; correlation coefficients between NDVI in summer and drought index values over a 3-month time scale gradually decreased; correlation coefficients with meteorological drought data for the 6-month time scale gradually increased; and their correlation coefficients with hydrological drought gradually increased. Correlation coefficients of NDVI with drought indicator values at 3 months gradually increased, as do those for meteorological drought at 6 months, while those for hydrological drought decreased slightly.

During spring, with increased temperature, snow melts in some areas of the Weihe River Basin, replenishing surface and groundwater. During this time, vegetation becomes more sensitive to changes in precipitation. During summer, with increased temperature, evapotranspiration in the basin increases, and vegetation responds to a greater extent to changes in precipitation and runoff. During fall, the various activities of vegetation decrease, demand for water decreases, and vegetation responses to changes in precipita-

tion and runoff also change. Meteorological and hydrological drought (SPI-3, SDI-3) at 3 months are more closely related to vegetation status (Figure 8). Meteorological drought at 3 months also correlated most with vegetation status in June, and hydrological drought at 3 months correlated most with vegetation status in May (Figure 2). Therefore, meteorological (SPI-3) and hydrological drought (SDI-3) data most closely related to changes in vegetation cover, and the impact lag time of 3 months was selected. Vegetation data for June were selected based on meteorological drought, and, for May, they were selected based on hydrological drought.
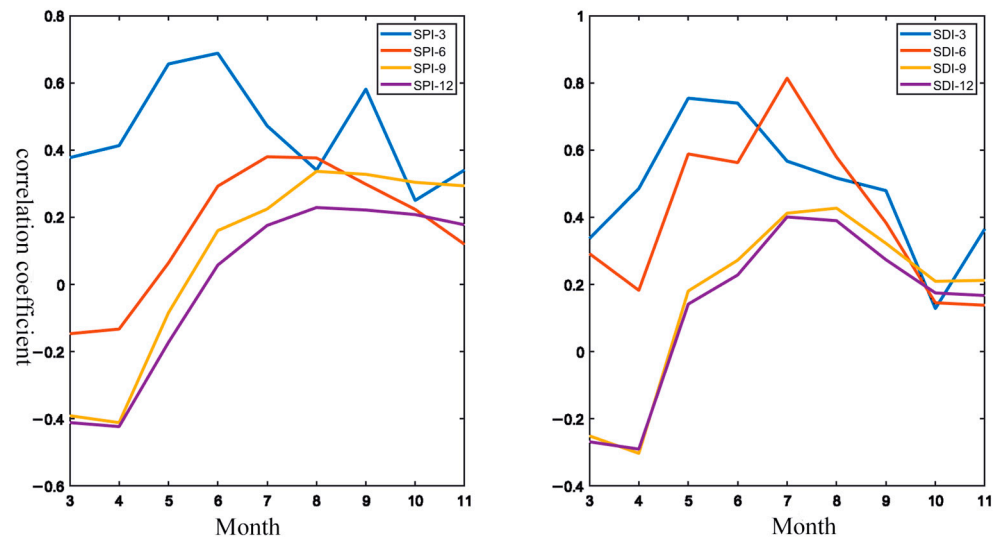
Figure 7. Line plots of correlations between drought and monthly scale NDVI at different time scales (3, 6, 9, and 12 months).
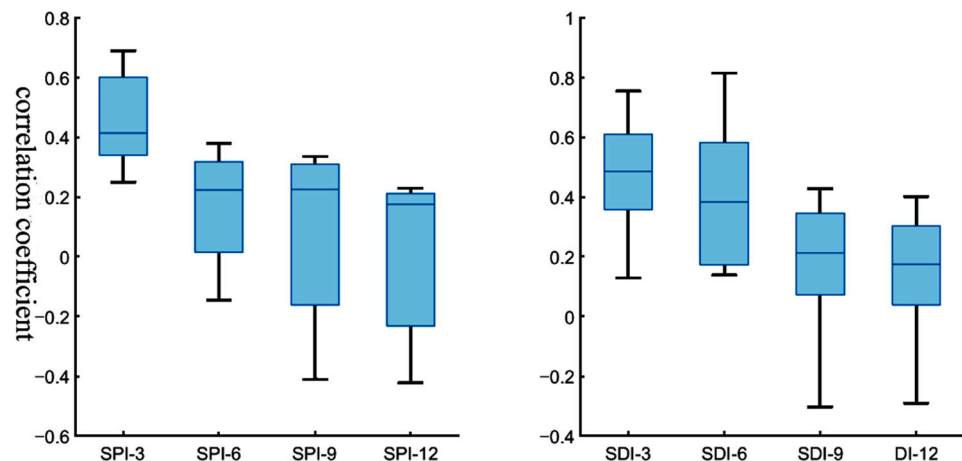

Figure 8. Boxplots of relationships between the effects of drought on vegetation during the growing season at different time scales (3, 6, 9, and 12 months).

5. Discussion

5.1. Impact of Drought Scenarios on Change in Vegetation Cover by Binary Copula Analysis Based on SPI–NDVI and SDI–NDVI

Based on correlation analysis between NDVI, SPI, and SDI data series corresponding to different time scales from 2001 to 2017, the lag in change in vegetation cover in response to drought at different time scales was obtained. Pearson's correlations between monthly NDVI data during the growing period and SPI and SDI data series for the scale with the largest correlation were obtained.

Meteorological or hydrological drought and the corresponding month's vegetation data were selected as four random variables (x, y, w, and z, respectively). MATLAB software (version R2021a) was used to make frequency histograms for each variable and to calculate their skewness and kurtosis (Figure 9, Table 3).
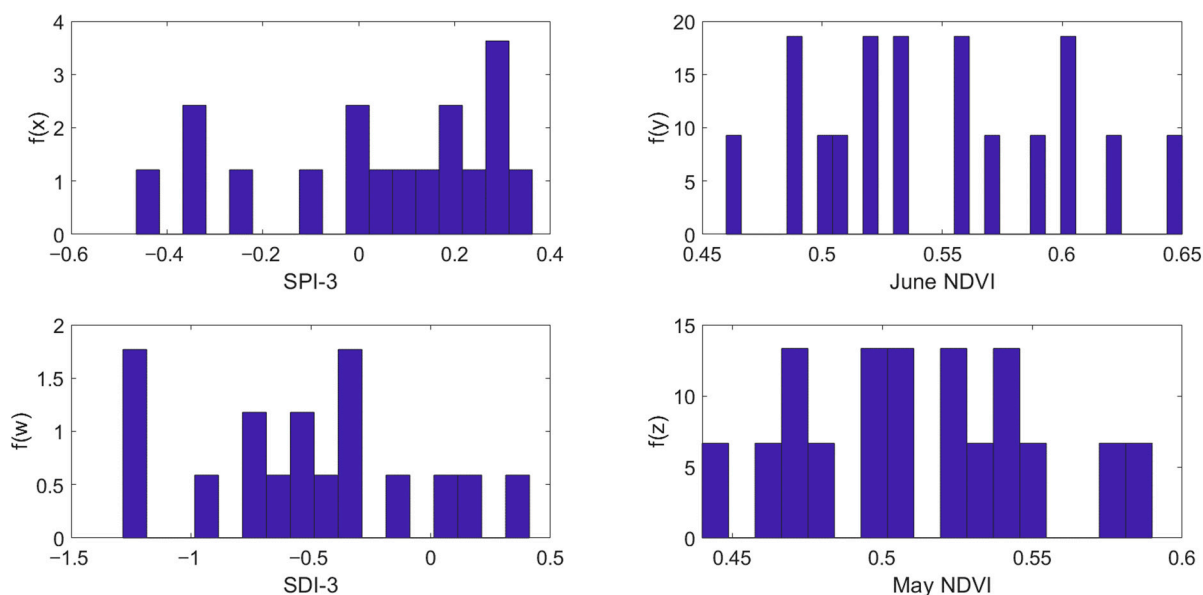

Figure 9. Frequency histograms for SPI-3, SDI-3, May NDVI, and June NDVI.

Table 3. Skewness and kurtosis of SPI-3, SDI-3, May NDVI, and June NDVI data.

Norm　　　　Variant	Skewness	Kurtosis
SPI-3	−0.63	2.17
June NDVI	0.28	2.17
SDI-3	0.08	2.44
May NDVI	0.16	2.42

Through the skewness and kurtosis of these four variables and frequency histograms, the distributions of the two are asymmetric. Normal, T-copula functions can be excluded to further analyze to determine the type of distribution of drought indicators and NDVI and to select the optimal copula function. We used a nonparametric method to estimate the overall distribution type (Figure 10).

Parameters θ and their rank correlation coefficients were calculated for three selected copula functions (Gumbel, Frank, and Clayton) (Table 4). Distribution function plots of these functions are presented in Figure 11, and density function plots are plotted in Figure 12.

Table 4. Parameters θ and corresponding rank correlation coefficients for three copula functions.

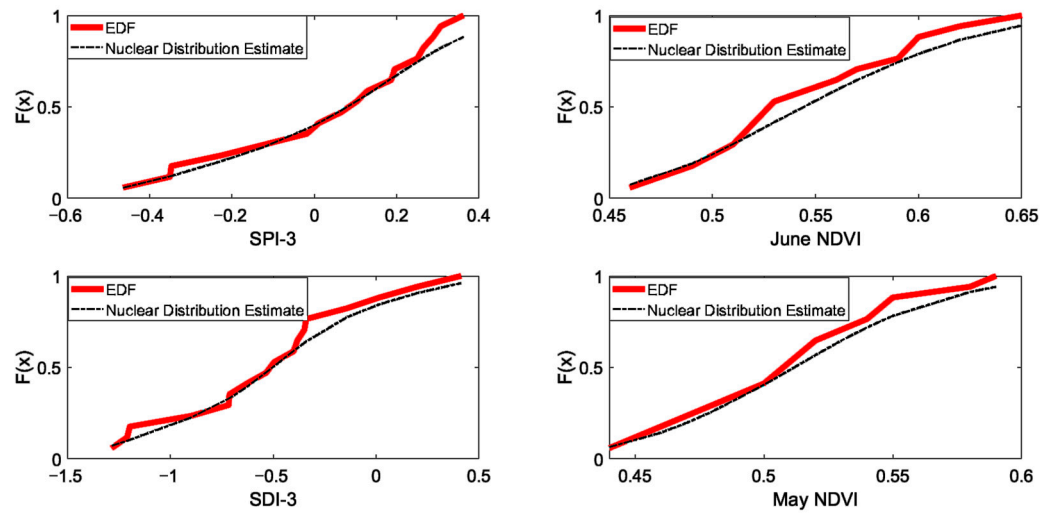| Parameter　　　　Function Type		Gumbel-Copula	Clayton-Copula	Frank-Copula
SPI-3 and June NDVI	θ	2.32	2.13	6.39
SDI-3 and May NDVI	θ	2.57	2.05	7.24
SPI-3 and June NDVI	Kendall	0.5685	0.5155	0.5338
SPI-3 and June NDVI	Spearman	0.76	0.70	0.73
SDI-3 and May NDVI	Kendall	0.61	0.51	0.57
SDI-3 and May NDVI	Spearman	0.80	0.69	0.77

Figure 10. Plots of empirical distribution functions and estimates of kernel distributions for SPI-3, SDI-3, May NDVI, and June NDVI.
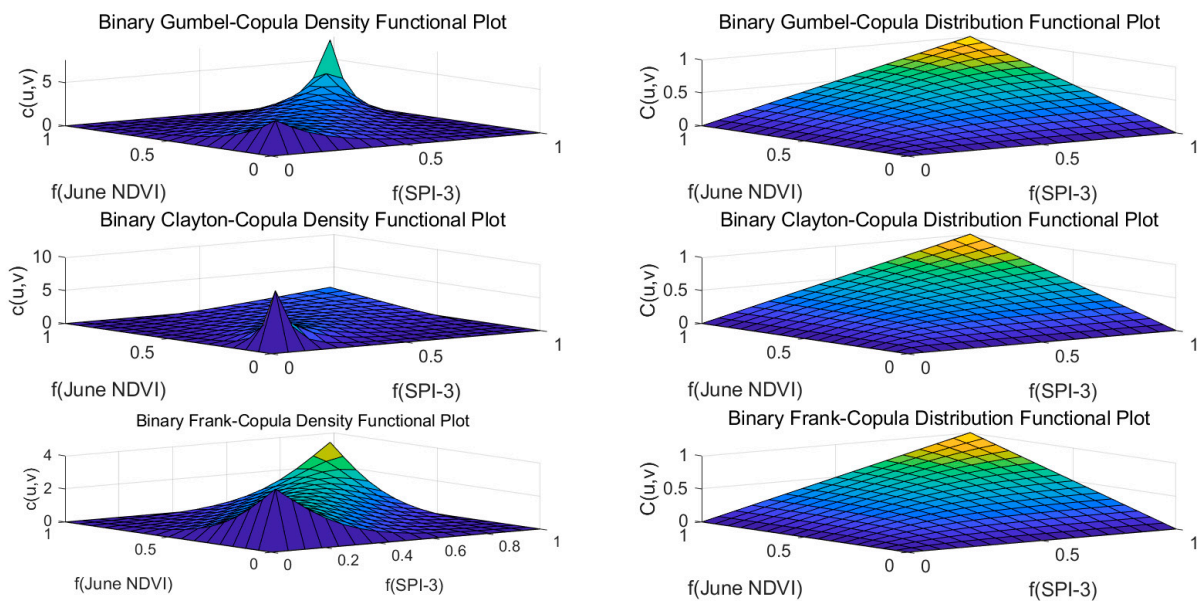

Figure 11. Density and distribution function plots of SPI-March and NDVI for June.

Taking the joint distribution of SPI-3 with June NDVI as an example, where the Kendall and Spearman coefficients of the Gumbel-copula function are 0.57 and 0.76, the Kendall and Spearman coefficients of the Clayton-copula function are 0.52 and 0.70, and the Kendall and Spearman coefficients of the Frank-copula function are 0.53 and 0.72, respectively. Similarly, the Kendall and Spearman coefficients of the Gumbel-copula function for the joint distribution of SDI-3 and May NDVI are 0.61 and 0.80, respectively. The Kendall and Spearman coefficients of the Clayton-copula function are 0.51 and 0.69, respectively, and the Kendall and Spearman coefficients of the Frank-copula function are 0.57 and 0.77, respectively. The Clayton-copula function appears to better fit the joint distribution of SPI-3 and June NDVI and SDI-3 and May NDVI. To confirm the optimal copula function, the three copula functions were tested for goodness-of-fit using the Akaike information criterion (AIC) (Table 5).
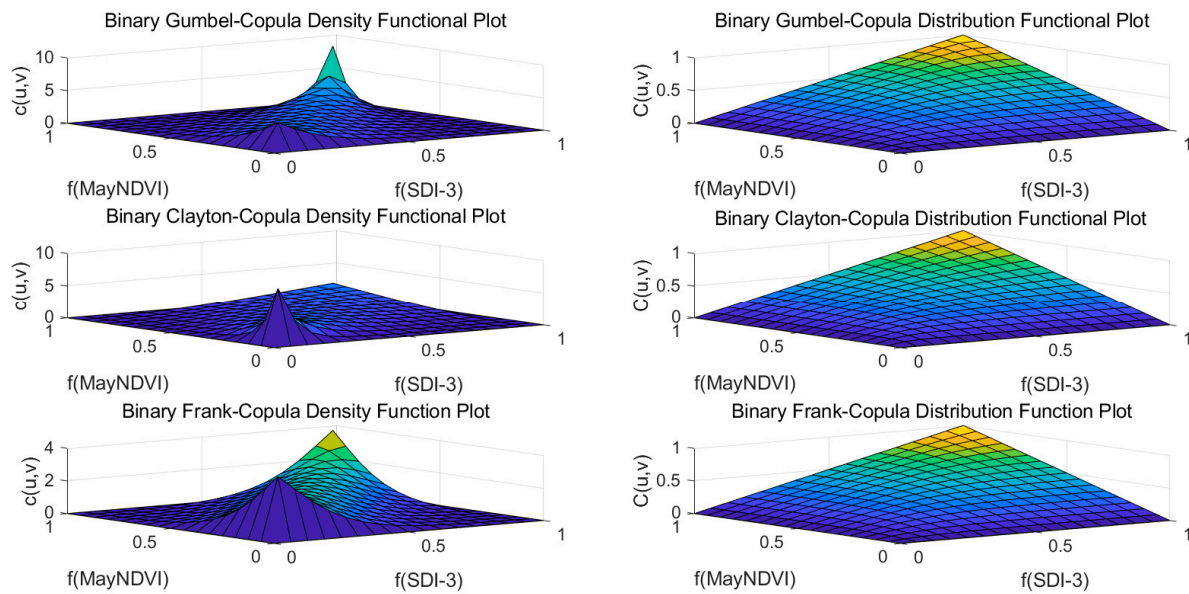
Figure 12. Density and distribution function plots of SDI-3 and NDVI for May.

Table 5. AIC test values for Gumbel-copula, Clayton-copula, and Frank-copula functions.

Joint Distribution	Function	AIC
	Gumbel-copula	-2.23×10^3
SPI-3 and June NDVI	Clayton-copula	-2.54×10^3
	Frank-copula	-1.85×10^3
	Gumbel-copula	-2.15×10^3
SDI-3 and May NDVI	Clayton-copula	-2.63×10^3
	Frank-copula	-1.96×10^3

AIC values of the Clayton-copula function are minimized for both types of joint distributions (-2.54×10^3 and -2.63×10^3, respectively). Therefore, the Clayton-copula function optimally fits the two types of joint distributions (Table 5).

We selected the Clayton-copula function to fit the two types of joint distributions of SPI and NDVI and SDI and NDVI. Relationships between drought and vegetation cover changes in the watershed under the joint distributions were analyzed based on corresponding density function plots (Figures 11 and 12). Probability density function plots of the Clayton-copula function are "L-shaped". The upper tail is low and the lower tail is high and thick (the correlation between drought and vegetation cover change is obvious). There is a high correlation between drought and change in vegetation cover when the probability is very small (in the case of a very small probability of hydrological and meteorological drought, there is a high probability of a very small change in vegetation cover). Based on correlations between drought and vegetation cover, the real-time drought situation can be used to predict vegetation cover. Therefore, it is convenient to take corresponding measures in advance to improve vegetation cover and avoid ecosystem damage.

5.2. Assessment of Changes in Vegetation Cover for Different Drought Stress Levels

Based on the response time of vegetation to drought, the corresponding correlation response models were constructed by selecting March SPI and June NDVI, and March SDI and May NDVI sequences using the optimal copula function. The probability of vegetation loss under different drought scenarios was deduced based on the joint distribution relationship.

Based on the derivation of Equations (15) and (16), the magnitude of the conditional probability of loss of vegetation condition < 0.50, 0.30, and 0.10 under different drought severities were calculated (Figures 13 and 14); average results are detailed in Tables 5 and 6. Changes in vegetation cover under different drought scenarios were assessed by quantifying the probability of loss of vegetation, which differed under different drought scenarios. The probabilities of loss of vegetation characterized by NDVI < 0.50, 0.30, and 0.10 preset points of extreme drought were 0.56, 0.33, and 0.21, respectively; values for severe drought were 0.48, 0.31, and 0.18, respectively, and those for moderate drought were 0.43, 0.25, and 0.14, respectively. For the hydrological drought scenario, the probabilities of vegetation loss characterized by NDVI < 0.50, 0.30, and 0.10 for extreme drought were 0.64, 0.45, and 0.29, respectively; these values are lower than those for the severe drought scenario (0.47, 0.30, and 0.17, respectively). We conclude that with intense drought, vegetation is more susceptible to influence, and the more obvious any change in vegetation cover will be. Additionally, vegetation status is more sensitive to hydrological than meteorological drought (hydrological drought more directly affects vegetation cover).
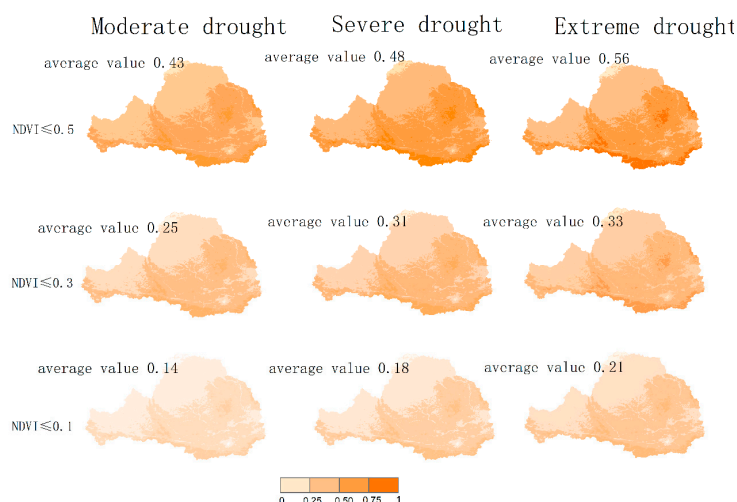

Figure 13. Probability of vegetation loss in June when vegetation cover at pre-determined points is < 0.5, 0.3, and 0.1 for different drought scenarios.
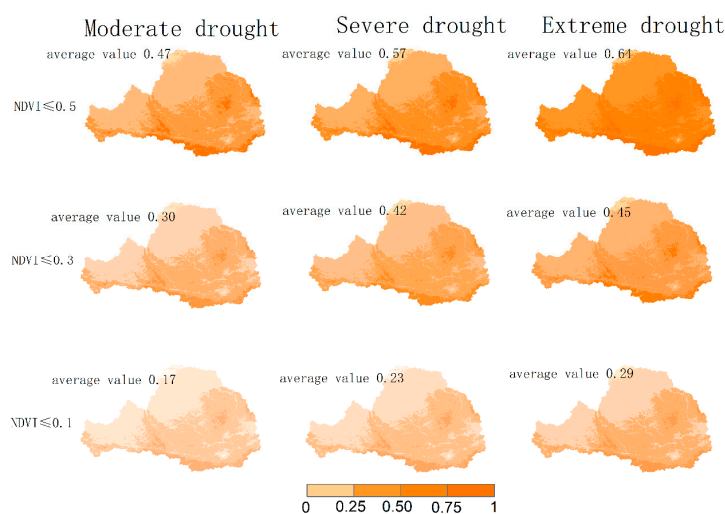

Figure 14. Probability of vegetation loss in May when vegetation cover at pre-determined points is < 0.5, 0.3, and 0.1 for different drought scenarios.

Table 6. Probability of vegetation loss under different drought stress levels.

Combination Scenarios	Meteorological Drought			Hydrological Drought		
	Moderate Drought	Severe Drought	Extreme Drought	Moderate Drought	Severe Drought	Extreme Drought
$NDVI \leq 0.5$	0.43	0.48	0.56	0.47	0.57	0.64
$NDVI \leq 0.3$	0.25	0.31	0.33	0.30	0.42	0.45
$NDVI \leq 0.1$	0.14	0.18	0.21	0.17	0.23	0.29

In terms of the probability of vegetation loss, the degree of drought impact is related to regional vegetation cover. For the probability of vegetation loss under different drought scenarios in the same area of Weihe River Basin, the probability of vegetation loss increases as the degree of drought intensifies (vegetation becomes more vulnerable, and when its status is below a predefined point, the probability of vegetation loss under drought stress decreases). The main Weihe River stream crosses the southern part of the watershed, with vegetation around it being mostly woodland and cultivated plants. Because of the proximity of vegetation to the river, cover in the southern part of the basin is larger and more sensitive to water changes. During droughts, the probability of vegetation loss in the southern watershed increases with drought intensification. The Luo River, meandering through the eastern sector of this basin, is flanked by cultivated flora and scrubland, bearing resemblance to the southern basin's landscape. Consequently, the likelihood of vegetation decline in this region escalates in tandem with the severity of drought conditions. We report that when vegetation is exposed to different degrees of drought at different pre-determined coverages, the probability of vegetation loss increases with drought severity. This demonstrates that the NDVI proposed by the Copula joint distribution has a certain lower-tailed correlation with SPI and SDI and that, when the latter two reach minimum values (when drought is most severe), the condition of smaller values of the NDVI of the NDVI of the normalized vegetation index probability is greater.

6. Conclusions

Utilizing MODIS MOD13A2 data along with SPI and SDI indices from 2001 to 2017, we analyzed the spatial and temporal patterns of NDVI and vegetation cover in the Weihe River Basin. A Copula function-based model was developed to assess vegetation loss under various drought conditions. Our main conclusions are as follows: (1) Over two decades, NDVI increased at a rate of 0.05 per decade, with a general upward trend in vegetation cover. NDVI values rose from north to south, with higher cover in the eastern and southern parts and lower in the western and northern regions. (2) No significant overall trend in vegetation cover change was observed, but an upward trend was noted in the northeast, central, and parts of the southwest and northwest areas (55.26% of the basin). Over time, regions with higher vegetation cover showed a decreasing trend, while those with lower cover showed an increasing one. (3) The southern and eastern parts of the basin were more susceptible to vegetation loss due to drought, with proximity to the river increasing sensitivity. The vegetation was more affected by hydrological drought than meteorological drought. The likelihood of vegetation loss increased with drought severity, but the probability of significant loss was lower at the same drought stress level.

Our analyses assist with the prediction of future changes in vegetation in response to drought events. As such, they will assist in monitoring and evaluating the benefits of ecological governance projects and levels of ecosystem restoration, and provide a basis and guidance for future ecological environment governance in this area.

Author Contributions: Conceptualization, F.W. and P.Z.; methodology, P.Z., F.W., Q.C. and B.X.; software, Q.C.; validation, H.L.; formal analysis, F.W. and P.Z.; investigation, B.X. and H.L.; resources, H.Y.; data curation, H.L.; writing—original draft preparation, F.W. and P.Z.; writing—review and editing, F.W., P.Z., Q.C., B.X., H.L. and H.Y.; visualization, H.Y. and X.H.; supervision, X.H.; project

References

1. Su, J.; Chen, D.; Zheng, D.; Su, Y.; Li, X. The insight of why: Causal inference in Earth system science. *Sci. China Earth Sci.* **2023**, *66*, 2169–2186. [CrossRef]
2. Anderegg, W.R.; Anderegg, L.D.; Berry, J.A.; Field, C.B. Loss of whole-tree hydraulic conductance during severe drought and multi-year forest die-off. *Oecologia* **2014**, *175*, 11–23. [CrossRef] [PubMed]
3. Li, J.; Xi, M.; Wang, L.; Li, N.; Wang, H.; Qin, F. Vegetation Responses to Climate Change and Anthropogenic Activity in China, 1982 to 2018. *Int. J. Environ. Res. Public Health* **2022**, *19*, 7391. [CrossRef] [PubMed]
4. Wang, Q.; Zhang, Q.P.; Zhou, W. Grassland Coverage Changes and Analysis of the Driving Forces in Maqu County. *Phys. Procedia* **2012**, *33*, 1292–1297. [CrossRef]
5. Zhou, S.; Wang, Y.; Chang, J.; Guo, A.; Li, Z. Study on the spatial pattern of spatial and temporal evolution of drought in the Yellow River Basin. *J. Hydraul. Eng.* **2019**, *50*, 1231–1241. [CrossRef]
6. Qu, Y.; Lv, J.; Sun, Z.; Sun, H.; Ma, M. Drought mitigation research review and outlook. *J. Hydraul. Eng.* **2018**, *49*, 115–125. [CrossRef]
7. Feng, S.; Hao, Z.; Zhang, X.; Wu, L.; Zhang, Y.; Hao, F. Climate change impacts on concurrences of hydrological droughts and high temperature extremes in a semi-arid river basin of China. *J. Arid Environ.* **2022**, *2022*, 104768. [CrossRef]
8. Chen, Q.; Timmermans, J.; Wen, W.; van Bodegom, P.M. A multi-metric assessment of drought vulnerability across different vegetation types using high resolution remote sensing. *Sci. Total Environ.* **2022**, *2022*, 154970. [CrossRef]
9. Wang, L.; Chen, W. A CMIP5 multimodel projection of future temperature, precipitation, and climatological drought in China. *Int. J. Climatol.* **2014**, *34*, 2059–2078. [CrossRef]
10. Liu, Y. Impacts of vegetation on drought trends. *Atmos. Sci.* **2016**, *40*, 156–412.
11. Inoubli, R.; Abbes, A.B.; Farah, I.R.; Singh, V.; Sattari, M.T. A review of drought monitoring using remote sensing and data mining methods. In Proceedings of the The 5th International Conference on Advanced Technologies for Signal and Image Processing (ATSIP'2020), Sousse, Tunisia, 2–5 September 2020.
12. West, H.; Quinn, N.; Horswell, M. Remote sensing for drought monitoring & impact assessment: Progress, past challenges and future opportunities. *Remote Sens. Environ. Interdiscip. J.* **2019**, *232*, 111291. [CrossRef]
13. AghaKouchak, A.; Farahmand, A.; Melton, F.S.; Teixeira, J.; Anderson, M.C.; Wardlow, B.D.; Hain, C.R. Remote sensing of drought: Progress, challenges and opportunities. *Rev. Geophys.* **2015**, *53*, 452–480. [CrossRef]
14. Zhang, S.; Zhu, X.; Liu, T.; Xu, K.; Guo, R. Response of gross primary production to drought under climate change in different vegetation regions of China. *Acta Ecol. Sin.* **2022**, *42*, 3429–3440.
15. Liu, Y. A numerical study on hydrological impacts of forest restoration in the southern United States. *Ecohydrology* **2011**, *4*, 299–314. [CrossRef]
16. Teuling, A.J.; Van Loon, A.F.; Seneviratne, S.I.; Lehner, I.; Aubinet, M.; Heinesch, B.; Bernhofer, C.; Grünwald, T.; Prasse, H.; Spank, U. Evapotranspiration amplifies European summer drought. *Geophys. Res. Lett.* **2013**, *40*, 2071–2075. [CrossRef]
17. Meng, X.H.; Evans, J.P.; McCabe, M.F. The impact of observed vegetation changes on land–atmosphere feedbacks during drought. *J. Hydrometeorol.* **2014**, *15*, 759–776. [CrossRef]
18. Leng, S.; Huete, A.; Cleverly, J.; Gao, S.C.; Yu, Q.; Meng, X.Y.; Qi, J.Y.; Zhang, R.R.; Wang, Q.F. Assessing the Impact of Extreme Droughts on Dryland Vegetation by Multi-Satellite Solar-Induced Chlorophyll Fluorescence. *Remote Sens.* **2022**, *14*, 1581. [CrossRef]
19. Zhou, Y.; Batelaan, O.; Guan, H.; Liu, T.; Duan, L.; Wang, Y.; Li, X. Assessing long-term trends in vegetation cover change in the Xilin River Basin: Potential for monitoring grassland degradation and restoration. *J. Environ. Manag.* **2023**, *349*, 119579. [CrossRef]
20. Mu, S.; Lee, K.; Chan, Y.; Gang, C.; Zhou, W.; Ju, W. Characteristics of spatial and temporal changes in vegetation cover in Inner Mongolia, 2001–2010. *Acta Geogr. Sin.* **2012**, *67*, 1255–1268.

21. Almouctar, M.A.S.; Yiping, W.; Fubo, Z. Drought analysis using normalized difference vegetation index and land surface temperature over Niamey region, the southwestern of the Niger between 2013 and 2019. *J. Hydrol. Reg. Stud.* **2024**, *52*, 101689–101701. [CrossRef]

22. Yin, Z.; Feng, Q.; Wang, L.; Chen, Z.; Chang, Y.; Zhu, R. Vegetation coverage change and its influencing factors across the northwest region of China during 2000–2019. *J. Desert Res.* **2022**, *42*, 11–21. [CrossRef]

23. Chen, J.; Shao, Z.; Huang, X.; Zhuang, Q.; Dang, C.; Cai, B.; Zheng, X.; Ding, Q. Assessing the impact of drought-land cover change on global vegetation greenness and productivity. *Sci. Total Environ.* **2022**, *852*, 158499. [CrossRef] [PubMed]

24. He, B.; Huang, L.; Chen, Z.; Wang, H. Weakening sensitivity of global vegetation to long-term droughts. *Sci. China Earth Sci.* **2018**, *61*, 60–70. [CrossRef]

25. Xu, C.; Mcdowell, N.G.; Fisher, R.A.; Wei, L.; Middleton, R.S. Increasing impacts of extreme droughts on vegetation productivity under climate change. *Nat. Clim. Chang.* **2019**, *9*, 948–953. [CrossRef]

26. Zuo, D.P.; Cai, S.Y.; Xu, Z.X.; Peng, D.Z.; Kan, G.Y.; Sun, W.C.; Pang, B.; Yang, H. Assessment of meteorological and agricultural droughts using in-situ observations and remote sensing data. *Agric. Water Manag.* **2019**, *222*, 125–138. [CrossRef]

27. Jiang, T.; Su, X.; Singh, V.P.; Zhang, G. Spatio-temporal pattern of ecological droughts and their impacts on health of vegetation in Northwestern China. *J. Environ. Manag.* **2022**, *305*, 114356. [CrossRef]

28. Guo, Y.; Huang, S.; Huang, Q.; Wang, H.; Wang, L.; Fang, W. Copulas-based bivariate socioeconomic drought dynamic risk assessment in a changing environment. *J. Hydrol.* **2019**, *575*, 1052–1064. [CrossRef]

29. Shi, X.; Ding, H.; Wu, M.; Zhang, N.; Shi, M.; Chen, F.; Li, Y. Effects of different types of drought on vegetation in Huang-Huai-Hai River Basin, China. *Ecol. Indic.* **2022**, *144*, 109428. [CrossRef]

30. Xu, H.; Zhu, Y.; Yagci, A.L.; Lü, H.; Gou, Q.; Wang, X.; Liu, E.; Ding, Z.; Pan, Y.; Liu, D.; et al. Development of composite drought indices for the coastal areas of southeastern China: A case study of Jinjiang and Jiulongjiang River basins. *J. Hydrol.* **2023**, *626*, 130210. [CrossRef]

31. Gumus, V.; Avsaroglu, Y.; Simsek, O.; Basak, A. Evaluating the duration, severity, and peak of hydrological drought using copula. *Theor. Appl. Climatol.* **2023**, *152*, 1159–1174. [CrossRef]

32. Poonia, V.; Jha, S.; Goyal, M.K. Copula based analysis of meteorological, hydrological and agricultural drought characteristics across Indian river basins. *Int. J. Climatol. A J. R. Meteorol. Soc.* **2021**, *41*, 4637–4652. [CrossRef]

33. Dixit, S.; Jayakumar, K.V. Spatio-temporal analysis of copula-based probabilistic multivariate drought index using CMIP6 model. *Int. J. Climatol. A J. R. Meteorol. Soc.* **2022**, *42*, 4333–4350. [CrossRef]

34. Zhao, J.; Huang, S.; Huang, Q. Copula-Based Abrupt Variations Detection in the Relationship of Seasonal Vegetation-Climate in the Jing River Basin, China. *Remote Sens.* **2019**, *11*, 1628. [CrossRef]

35. Zhao, J.; Li, G.; Lin, H.; Wang, Y.; Yu, Y.; Chu, G.; Zhang, J. Soil moisture response to rainfall on the Chinese Loess Plateau after a long-term vegetation rehabilitation. *Hydrol. Process.* **2018**, *32*, 1738–1754. [CrossRef]

36. Zhang, J.; Zhao, P.; Zhang, Y.; Cheng, L.; Song, J.; Fu, G.; Wang, Y.; Liu, Q.; Lyu, S.; Qi, S.; et al. Long-Term Baseflow Responses to Projected Climate Change in the Weihe River Basin, Loess Plateau, China. *Remote Sens.* **2022**, *14*, 5097. [CrossRef]

37. Wang, W.; Song, J.; Zhang, G.; Liu, Q.; Guo, W.; Tang, B.; Cheng, D.; Zhang, Y. The influence of hyporheic upwelling fluxes on inorganic nitrogen concentrations in the pore water of the Weihe River. *J. Ecol. Eng. J. Ecotechnol.* **2018**, *112*, 105–115. [CrossRef]

38. Deng, L.; Chen, J.; Fan, W.; Li, Y.; Shi, L. The Dynamic Response Characteristics of a Water Transmission Pipe Crossing a Loess Fault Using a Large-Scale Shaking Table Test: A Case Study. *Int. J. Geomech.* **2024**, *24*, 05023012. [CrossRef]

39. Li, M. Research on Remote Sensing Estimation Methods for Vegetation Cover. Master's Thesis, Chinese Academy of Sciences, Beijing, China, 2003.

40. Cheng, F.; Liu, S.; Yin, Y.; Lv, Y.; An, N.; Liu, X. The dynamics and main driving factors of coastal vegetation in Guangxi based on MODIS NDVI. *Ecol. Lett.* **2017**, *37*, 788–797.

41. Sun, C.; Bai, X.; Wang, X.; Zhao, W.; Wei, L. Response of vegetation variation to climate change and human activities in the Shiyang River Basin of China during 2001–2022. *J. Arid Land* **2024**, *16*, 1044–1061. [CrossRef]

42. He, B.; Ding, J.; Zhang, Z.; Ghulam, A. Experimental analysis of spatial and temporal dynamics of fractional vegetation cover in Xinjiang. *Acta Geogr. Sin.* **2016**, *71*, 1948–1966.

43. McKee, T.B.; Doesken, N.J.; Kleist, J. The relationship of drought frequency and duration to time scales. In Proceedings of the 8th Conference on Applied Climatology, Anaheim, CA, USA, 17–22 January 1993; pp. 179–183.

44. Nalbantis, I.; Tsakiris, G. Assessment of Hydrological Drought Revisited. *Water Resour. Manag.* **2009**, *23*, 881–897. [CrossRef]

45. Nalbantis, I. Evaluation of a hydrological drought index. *Eur. Water* **2008**, *23*, 67–77.

46. Zhao, P.; Lu, H.; Wang, W.; Fu, G. From meteorological droughts to hydrological droughts: A case study of the Weihe River Basin, China. *Arab. J. Geosci.* **2019**, *12*, 364. [CrossRef]

47. Zhao, P.; Xie, B.; Huang, X.; Qu, B. The dynamic change of propagation from meteorological drought to hydrological drought at the basin scale: Acase study from the Weihe River Basin, China. *Front. Environ. Sci.* **2022**, *10*, 1054975. [CrossRef]

48. Kao, S.-C.; Govindaraju, R.S. A copula-based joint deficit index for droughts. *J. Hydrol.* **2010**, *380*, 121–134. [CrossRef]

49. Li, J.; Peng, T.; Dong, X.; Li, Z.; Wang, G.; Chang, W.; Lin, Q.; Wang, J. Study on hydrological drought risk in Han River basin based on Copula function. *Soil Water Conserv. Res.* **2022**, *29*, 179–188.

50. Li, Z.; Li, X.; Zhang, D.; Lin, Y. Copula-based probability analysis of hydrological drought in the Dongting Lake-basin-Yangtze River system. *Lake Sci.* **2022**, *34*, 1319–1334.

51. Sklar, M. *Fonctions de Répartition à n Dimensions et Leurs Marges*; Publications de l'Institut de Statistique de l'Universite de Paris: Paris, France, 1959; pp. 229–231.
52. Herr, H.D.; Krzysztofowicz, R. Generic probability distribution of rainfall in space: The bivariate model. *J. Hydrol.* **2005**, *306*, 234–263. [CrossRef]
53. Li, C.; Singh, V.P.; Mishra, A.K. A bivariate mixed distribution with a heavy-tailed component and its application to single-site daily rainfall simulation. *Water Resour. Res.* **2013**, *49*, 767–789. [CrossRef]
54. Kong, X.; Huang, G.; Fan, Y.; Li, Y. Maximum entropy-Gumbel-Hougaard copula method for simulation of monthly streamflow in Xiangxi river, China. *Stoch. Environ. Res. Risk Assess.* **2015**, *29*, 833–846. [CrossRef]
55. Hürlimann, W. Fitting bivariate cumulative returns with copulas. *Comput. Stat. Data Anal.* **2004**, *45*, 355–372. [CrossRef]
56. Genest, C.; Rivest, L.-P. Statistical inference procedures for bivariate Archimedean copulas. *J. Am. Stat. Assoc.* **1993**, *88*, 1034–1043. [CrossRef]
57. Massey, F.J., Jr. The Kolmogorov-Smirnov test for goodness of fit. *J. Am. Stat. Assoc.* **1951**, *46*, 68–78. [CrossRef]